Coupling magma ascent models with volatile diffusion chronometry

Olivier Bernard, Fidel Costa Rodriguez

Earth Planet. Sci. Lett. 648 (2024) 119099

Contents lists available at ScienceDirect

Earth and Planetary Science Letters

journal homepage: www.elsevier.com/locate/epsl

Coupling magma ascent models with volatile diffusion chronometry

O. Bernard *, F. Costa

Institut de Physique du Globe de Paris, CNRS, Université Paris Cité, 1 Rue Jussieu, Paris 75005, France

ARTICLE INFO

Editor: Dr C. M. Petrone

Keywords:
Magma ascent
Diffusion chronometry
Volatiles
Conduit modelling
Eruption dynamics
Melt embayments

ABSTRACT

The pre- and syn-eruptive magma decompression rate is recognized as a key parameter modulating eruption dynamics, with explosive eruptions being generally associated with much larger decompression rates than effusive ones. Magma decompression rates cannot be directly measured and thus are typically inferred from petrological, geochemical, numerical modelling, and seismic data. Most studies use petrological information of volatile element diffusive equilibration in glass and crystals to infer a single value for the magma ascent rate for a given eruption, even though numerical volcano conduit simulations show that changes of velocity are expected during magma ascent. Here we integrate magma ascent conduit models with diffusion chronometry of volatiles in melt embayments and phenocrysts to obtain a more comprehensive understanding of magma ascent rates. We find that incorporating a more realistic boundary condition that depends on the magma ascent path with variable velocities gives time estimates that can be up to a factor of 7 longer than from the standard assumption of constant magma ascent rate. Therefore, previous magma ascent rates from diffusion chronometry of volatiles in crystals and melts with a fixed boundary condition may be significantly overestimated. Overall, we show that coupling of magma ascent models with diffusion chronometry can provide more robust inferences of magma ascent and thus improve the understanding of the role of this parameter into the explosive and effusive eruption controls.

1. Introduction

The magma ascent rate is widely recognized as a key parameter controlling the dynamics of volcanic eruptions (Gonnermann and Manga, 2013; Cassidy et al., 2018). Despite some exceptions, petrological and experimental studies suggest that large explosive eruptions tend to result mostly from fast magma ascent from intermediate to shallow reservoir in a matter of minutes to seconds (Toramaru, 2006; Humphreys et al., 2008; Shea et al., 2010; Houghton et al., 2010), whereas effusive eruptions arise from slower ascent of generally more degassed magmas (Rutherford and Hill, 1993; Hammer and Rutherford, 2002; Castro et al., 2013; Cassidy et al., 2015). There are several methods to estimate magma velocities, including seismicity to track magma migration (Endo and Murray, 1991; Caudron et al., 2018), decompression experiments to reproduce observations on natural products (Martel, 2012; Shea and Hammer, 2013) or to calibrate models to be applied on natural products' textures (Toramaru, 2006; Toramaru et al., 2008), and methods based on the timescales of chemical reequilibration of volatile species in crystals or melts because of decompression (Liu et al., 2007; Charlier et al., 2012; Costa, 2021). This variety of methods has been used to estimate magma ascent rates for effusive and mildly explosive activity (Lloyd et al., 2014; Barth et al., 2019; Bernard and Bouvet de Maisonneuve, 2020; Newcombe et al., 2020a) to cataclysmic eruptions (Toramaru, 2006; Shea et al., 2010; Nguyen et al., 2014; Myers et al., 2018, 2021; Valdivia et al., 2021; Geshi et al., 2021). Estimates of ascent rates have been obtained for mafic (Chen et al., 2013; Ferguson et al., 2016; Moussallam et al., 2019; Thivet et al., 2020; Zuccarello et al., 2022), intermediate (Toramaru et al., 2008; Romano et al., 2020; Cutler et al., 2022; Bernard et al., 2022a) and highly-evolved magma compositions (Liu et al., 2007; Alfano et al., 2012; Martel, 2012; Myers et al., 2018; Elms et al., 2023).

However, most if not all previous studies infer a single value for the magma ascent rate. It is unclear whether this rate corresponds to the mean, a maximum or minimum value and it seems to imply a constant magma ascent rate from the last storage zone to the surface. Moreover, magma ascent rates calculated by various methods rely on different proxies and as such, they typically do not quantify the same process. Seismic methods for instance typically reflect on the magma migration and therefore be applicable only during the opening of a new dike or conduit (Caudron et al., 2018). Textural methods such as vesicle number

* Corresponding author.
E-mail address: obernard@ipgp.fr (O. Bernard).

https://doi.org/10.1016/j.epsl.2024.119099
Received 7 August 2024; Received in revised form 21 October 2024; Accepted 28 October 2024
Available online 8 November 2024

density give a snapshot of the ascent rate when the bubble reaches the size, shape and distribution they have at the time we sample the deposit so, closer to fragmentation in case of homogeneous nucleation (Toramaru, 2006; Shea, 2017). For the case of methods based on diffusion chronometry, obtaining a single value for magma ascent would imply the decompression rate to be an average value during the time the element of interest is either leaving the crystal phase or exsolving from the melt (Harris et al., 2024). The result is that, for a given eruption, estimated magma decompression rate can vary by several orders of magnitude depending on the method chosen (Fig. 1; i.e. calculations for Mt St-Helens 1980 eruption span 5 order of magnitude - Rutherford and Hill, 1993; Geschwind and Rutherford, 1995; Toramaru, 2006; Humphreys et al., 2008), while if a similar method is used independently by a different team on different deposits of the same eruption, similar numbers are found (i.e. Llaima Curacautín eruption – Valdivia et al., 2021; Bernard et al., 2022a).

Another view point of magma ascent are the results of numerical simulations which show that due to volatile exsolution and expansion the density of the magma decreases upon decompression and thus its velocity towards the surface changes in a non-linear manner (Mastin, 2002; Kozono and Koyaguchi, 2009; Degruyter et al., 2012; La Spina et al., 2015; Campagnola et al., 2016, 2021). This is even the case for the most simplistic situation where magma would ascend in one step from the final storage zone to the surface in the case of an ongoing and steady Hawaiian or Plinian eruption.

A few studies have coupled numerical models with natural data to obtain magma decompression rates. Su and Huber (2017), Barth et al. (2019) found that a higher degree of non-linearity of the ascent path tended to decrease the magma decompression rate obtained by volatile diffusion chronometry. Similarly, Hajimirza et al. (2021) reconciled bubble number density with other independent geospeedometers with the help of numerical models to show that both could give similar results in the case of heterogeneous bubble nucleation on magnetite. However, these studies did not directly link their diffusion models to more realistic models of magma ascent in a conduit.

In this contribution we aim at exploring the impact and usefulness of coupling numerical simulations of magma ascent with inferences of magma transfer time from diffusion chronometry studies of volatiles in melt embayments and crystals. We first review the importance of boundary conditions in volatile diffusion chronometry on the calculated magma ascent rate. Then we build a framework to couple diffusion chronometry with a non-linear magma ascent path derived from conduit numerical modelling. We explore the effect of this boundary condition on diffusion modelling of H_2O and CO_2 in glass embayment and on the resulting estimated magma decompression rate and concentration profile. We find that considering a non-constant magma ascent may have a strong effect on the diffusion-based calculated timescales of ascent. This implies that similar non-linear magmatic processes could also have a strong impact on other diffusion chronometers and the timescales we derive from them.

2. Methods

We note that most diffusion chronometry studies from the literature report the magma ascent rate rather than magma decompression rate. However, the original calculations provide the time from which a rate is obtained using a storage pressure obtained from geobarometers and/or volatile saturation models which are converted into magma storage depth using a density model. Given that there are several unknowns about the density of the crust and/or the density of the magma column, we typically report our results in terms of magma decompression rate rather than ascent rate with the understanding that the latter can be

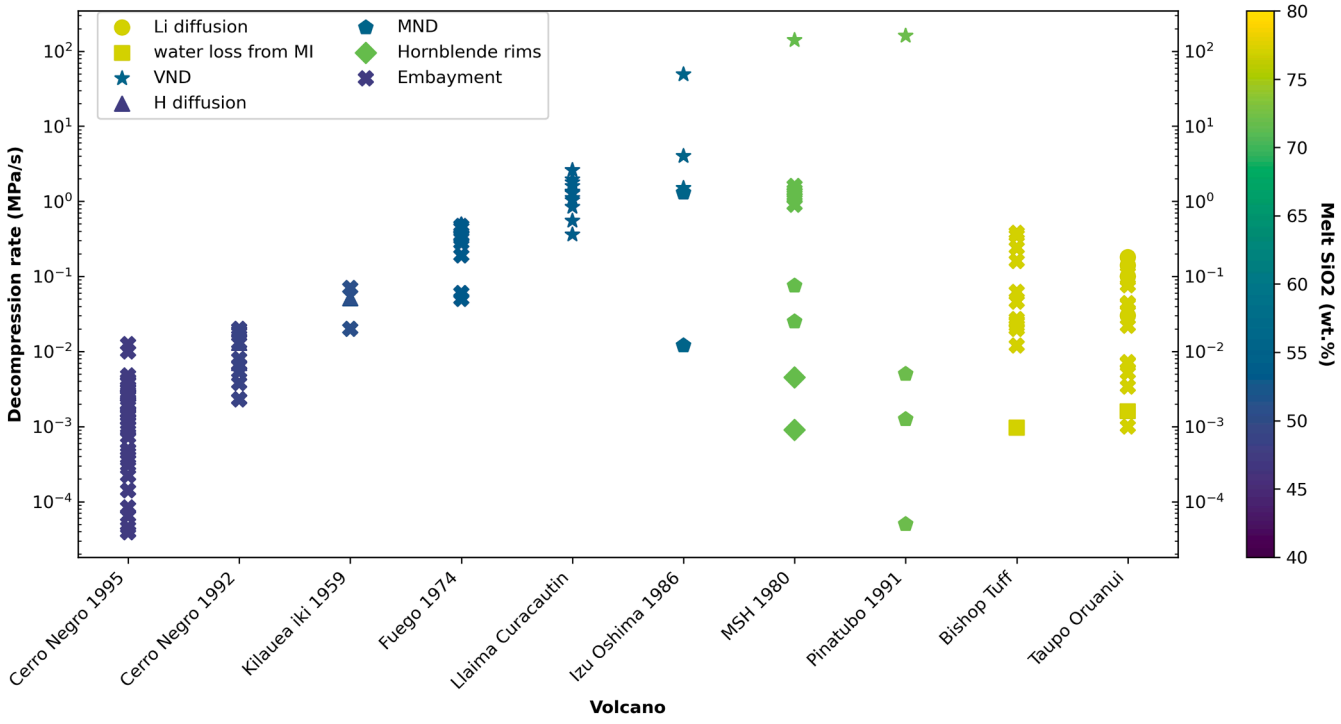

Fig. 1. Magma decompression rate estimates from the literature for various eruptions across a wide compositional range. The magma decompression rates have been estimated using different methods and/or by different authors. Methods include MND (Microlite number density) water exsolution rate meter (Toramaru et al., 2008), H diffusion in Olivine, VND (Vesicle number density) water exsolution rate meter (Toramaru, 2006), Hornblende breakdown rims (Rutherford and Devine, 2003), volatile diffusion in embayment, Lithium diffusion in plagioclase, water loss from MI (melt inclusions). Cerro Negro 1995 and 1992, (Barth et al., 2019; Newcombe et al., 2020a); Kilauea Iki 1959, (Ferguson et al., 2016; Newcombe et al., 2020b; 2020a); Fuego 1974, (Lloyd et al., 2014; Newcombe et al., 2020a); Llaima Curacautín, (Valdivia et al., 2021; Bernard et al., 2022a); Izu-Oshima 1986, (Toramaru, 2006; Toramaru et al., 2008); Mt St-Helens 1980, (Rutherford and Hill, 1993; Geschwind and Rutherford, 1995; Toramaru, 2006; Humphreys et al., 2008); Pinatubo 1991, (Hammer and Rutherford, 2002; Toramaru, 2006); Bishop Tuff, (Myers et al., 2018; 2019); Taupo Oruanui, (Charlier et al., 2012; Liu et al., 2007; Myers et al., 2018; 2019).

obtained from the former using a density model.

2.1. Eruptions of interest

We explore the differences between using a constant decompression rate and a non-linear decompression rate in models of diffusion chronometry for volatiles in melt embayments and crystals. For this we use a combination of forward diffusion chronometry and magmatic volatile saturation models on 13 well-studied eruptions from the literature (Table 1). These have a wide range in magma composition, they all are explosive eruptions and some have had major societal impacts. We use the physical parameters obtained from previous publications (Table 1 and supplementary) as inputs in the volatile saturation models (steps explained in the following paragraph).

2.2. Diffusion chronometry

Diffusion chronometry was used to calculate the timescales from the re-equilibration of chemical gradients of volatile elements in volcanic minerals and/or glass, generated by the changing environmental conditions during a magmatic process (Costa et al., 2008, 2020; Costa and Morgan, 2010; *and references therein*). Volatile elements are exsolved from the melt in response to pressure drop during magma ascent, and thus these produce gradients in compositions in the melt that can be used to obtain magma ascent times from which we can derive magma decompression rates (Liu et al., 2007; Fig. 2).

Here, we investigate the diffusion of H_2O and CO_2 - two volatile species that have been extensively studied for melt physical parameters. Several studies have focused on calibrating the necessary parameters such as the diffusion coefficient or the partition coefficient between different phases (Zhang and Behrens, 2000; Behrens et al., 2004; Liu et al., 2007; Barth et al., 2023; Towbin et al., 2023), as well as the influence changes in the initial conditions such as temperature, initial pressure and concentrations can have on the obtained timescales (Mutch et al., 2019; Ostorero et al., 2022; Bernard et al., 2022b). However, an important aspect that needs to be explored further is how volatile contents in the melt change as magma moves towards the surface which inherently depends on the decompression rate. Such changes drive diffusion in the melt and crystal and thus have a direct impact on the calculated times and ascent rates. In most studies, a classical H_2O and CO_2 dissolution profile based on solubility models has been used (Newman and Lowenstern, 2002; Liu et al., 2005), whereas in others that studied volatiles whose behaviour in melts upon decompression is less known (e.g., halogens), a single-step decompression assumption has been used (i.e. F-Cl-OH in apatite – Li et al., 2020; Bernard et al., 2022b). Here we address a more complex and realistic scenario where diffusion of volatiles (H_2O and CO_2) is driven by the output from physical conduit models of magma ascent which is non-linear and thus produces non-linear changes of volatile concentrations in the melt.

2.3. Diffusion of H_2O–CO_2 in the melt

We solved the 1-dimensional expression of Fick's 2nd law with finite difference forward scheme (Eq. (1)), to produce H_2O and CO_2 diffusion models:

$$\frac{\partial C_{x,t}}{\partial t} = \frac{\partial}{\partial t}\left(D_{x,t}\frac{\partial C_{x,t}}{\partial x}\right) \tag{1}$$

Where C is the H_2O or CO_2 concentration at a time t and a position x along the profile and D is the H_2O or CO_2 diffusion coefficient at a time t and a position x. As H_2O and CO_2 diffusion in the melt are interdependent, we calculated D_{H_2O} and D_{CO_2} using the formulation calibrated for all silicate melts of Behrens et al. (2004) - note that in the original paper, there is a typo in the expression of D_{H_2O} (5.73 $\times P$ instead of 57.3 $\times P$ – Zhang et al., 2007):

$$D_{H2O} = X \times \exp(m) \times \left(1+\exp\left(56+m+X\times\left(-34.1+\frac{44620}{T}+\frac{57.3\times P}{T}\right)-\sqrt{X}\times\left(0.091+4.77\times\frac{10^6}{T^2}\right)\right)\right) \tag{2}$$

and:

$$D_{CO2} = exp\left(-8.20-\frac{22963+2.005\times P}{T}+C_{H2O}\times\left(1.4262+\frac{2416.1}{T}\right)\right)\times 10^{12} \tag{3}$$

where:

$$m = -20.79-\frac{5030}{T}-\frac{1.4\times P}{T}, \tag{4}$$

and:

$$X = \frac{\frac{C_{H2O}}{18.015}}{\frac{C_{H2O}}{18.015}+\frac{C_{CO2}}{440100}+\frac{(100-C_{CO2}-0.0001\times C_{CO2})}{32.49}}, \tag{5}$$

Where T is the temperature in Kelvin, P is the pressure in bars, C_{H2O} is the melt water concentration in wt. %, and C_{CO2} is the melt CO_2 concentration in ppm. With this formulation, H_2O and CO_2 diffusion coefficients are interdependent and need to be solved simultaneously.

Table 1
Details of the eruptions used to model magma decompression rates ([a]Global Volcanism Program, Smithsonian institution; [b]Costantini et al., 2010; [c]Marshall et al., 2022; [d]Hildreth and Wilson, 2007; [e]Wilson et al., 2006; [f]Garcia et al., 2000) and starting conditions (P, T, H_2O and CO_2) used in the saturation model and the diffusion model for each eruption. P_i is the initial pressure used in our simulations and based on literature pre-eruptive storage pressures. References are reported in the supplementary table for each volcano.

Volcano	Eruption year	Eruption style	VEI	Melt composition	T (°C)	P_i (MPa)	H_2O initial (wt. %)	CO_2 initial (ppm)
Kilauea	1992	Hawaiian	2[f]	Basalt	1150	55	0.75	400
Etna	122 BCE	Plinian	5[a]	Basalt	1060	160	2.87	585
Masaya	60 ka BP – Fontana Lapilli	Plinian	5[b]	Basaltic andesite	1100	60	1.8	110
Llaima	13.3 ka BP - Curacautín	Plinian	6[c]	Basaltic andesite	1050	200	2.7	1000
Vesuvius	79 CE - Pompeii	Plinian	5[a]	Phonolite	850	150	6.0	100
Rabaul	2006	Sub-Plinian	4[a]	Trachydacite	975	100	2.8	150
Samalas	1257 CE	Plinian	7[a]	Trachydacite	930	100	4.2	20
Santorini	3600 BP – Late Bronze Age	Plinian	7[a]	Rhyolite	850	175	5.4	200
Mt St Helens	1980	Plinian	5[a]	Rhyolite	880	200	5.5	100
Chaiten	2008	Plinian	5[a]	High-silica Rhyolite	800	120	4.0	20
Pinatubo	1991	Plinian	6[a]	High-silica Rhyolite	780	220	6.4	20
Long Valley	760 ka BP – Bishop Tuff	Plinian	7[d]	High-silica Rhyolite	740	150	5.0	200
Taupo	25.7 ka BP - Oruanui	Plinian	8[e]	High-silica Rhyolite	780	90	3.5	75

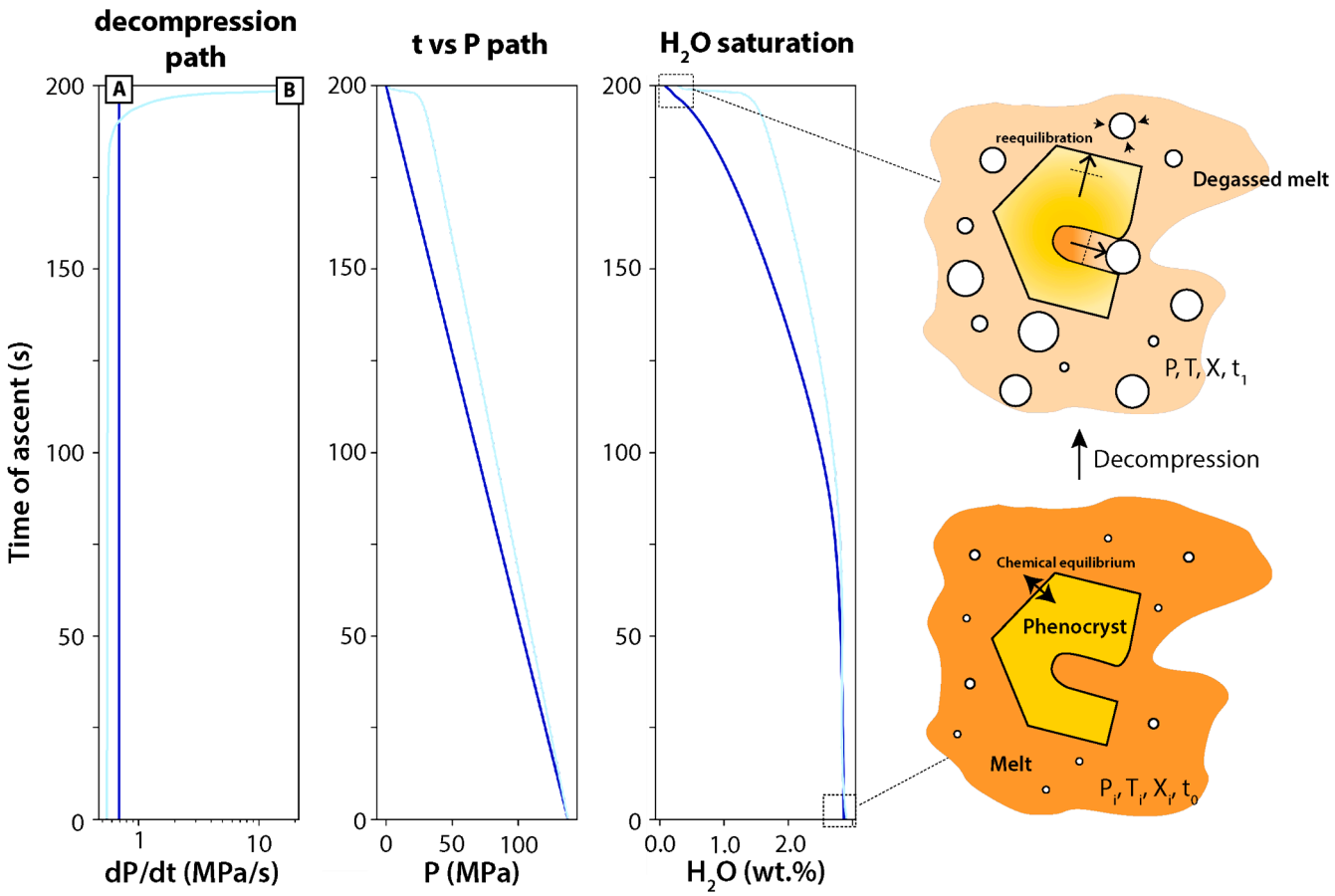

Fig. 2. Illustration of the effect of the decompression path on the H_2O saturation profile that will serve as the outside boundary condition in diffusion modelling. Path A (lines in bright colour) is the result of using a single value for magma ascent rate and B (lines in light blue) is a result of a numerical simulation where the rate changes during ascent. Both paths have the same average dP/dt, initial and final pressure and duration. The sketch represents the effect of decompression on the volatiles that are exsolved from the melt to the fluid phase (bubbles here). Because of various diffusion speeds between the phases (melt pockets, phenocrysts), volatile concentration gradients are formed due to rapid decompression preventing reequilibration. P_i, T_i, X_i: initial pressure, temperature and melt chemical composition, P_f, T_f, X_f: final pressure, temperature and melt chemical composition. t_0 and t_1 are the starting and ending time between which diffusion of volatiles in the melt occurs.

2.4. Boundary conditions for diffusion chronometry

We solved the diffusion Eq. (1) numerically using a finite difference forward scheme. To do this we need to define: (a) the initial conditions which correspond to the volatile concentration profile in the melt or crystal $C_{t=0,\ x>0} = C_{initial}$ and for which we considered a homogenous concentration, and (b) the boundary conditions, which is how the volatile concentration varies at the boundary ($x = 0$) between the crystal and the melt, or the melt and bubble, expressed as $C_{t>0,\ x=0} = C_{boundary}$. The boundary conditions can be considered constant or varying with time, and the manner in which they are defined imply different magma ascent scenarios as described below.

The case of a constant boundary condition can be defined as: $C_{t>0,x=0} = C_{P_{final}}$ with $C_{P_{final}}$ being the concentration at the final equilibrium pressure which depends solely on the chosen volatile saturation model (see the following paragraph). This is a simplistic model as it implies that magma rose instantaneously from the initial pressure at $t = 0$ to the final pressure at $t > 0$. A second case is to use a pressure-dependent volatile saturation model and extract a volatile concentration at the boundary as a function of pressure:

$$C_{t>0,\ x=0} = C\left(\frac{dP}{dt} = Constant,\ P,\ T, X\right) \tag{6}$$

This is commonly used in volatile diffusion chronometry to estimate magma ascent rates in the literature (Liu et al., 2007; Humphreys et al., 2008; Lloyd et al., 2014; Moussallam et al., 2019; Myers et al., 2018, 2021; Elms et al., 2023; Hosseini et al., 2023). The saturation model gives the equilibrium volatile concentration at a given pressure depending on the initial storage temperature T and melt composition X. This is more accurate than a single-step model and is also well constrained for H_2O and CO_2 as several well-defined saturation models exist. However, this model is also a simplification of the problem, as it uses a constant decrease of pressure as a function of time, and thus a constant ascent rate (Fig. 2). An improved version of this model has recently been developed by using a two-step decompression rate (Harris et al., 2024). A way to further improve on this, is to set a boundary condition where the concentration changes in a non-linear fashion due to a varying decompression rate. In our approach, this is given by the output of a magma ascent conduit model (see the following sections):

$$C_{t>0,\ x=0} = C\left(\frac{dP}{dt} = Conduit\ model,\ P,\ T, X\right) \tag{7}$$

In this way the pressure path is linked to physical constraints of the conduit models (see paragraph 2.5 for details; Fig. 2). For all the modelled cases we assumed that the volatile concentration in the fluid phase is at all times in equilibrium with the volatile concentration in the melt/crystal, which may as well be a simplification but it is a common approach in the literature (Humphreys et al., 2008; Moussallam et al., 2019; Myers et al., 2018, 2021; Newcombe et al., 2020a; Elms et al., 2023; Harris et al., 2024).

2.5. Volatile saturation models

To obtain the dissolved H_2O and CO_2 concentrations in the melt as a function of pressure, temperature, and composition we used the mixed fluid saturation model MagmaSat (Ghiorso and Gualda, 2015) for all the 13 eruptions, with a 1 MPa pressure step and representative melt composition, storage temperature and pressure as well as initial volatile content mined from the literature (Table 1).

2.6. Magma ascent and conduit models

To calculate the changes at the boundary of the melt embayment or crystals during non-linear decompression and ascent, we used physically-based models that simulate the changes of magma physical properties (P, T, density, viscosity, volatile content, etc.) throughout its ascent in the volcanic conduit (La Spina et al., 2015; Campagnola et al., 2016). These simulations use a set of initial parameters (i.e., melt chemistry, initial volatile content, storage pressure and temperature, vesicle number density, etc.) that we derive from previous petrological

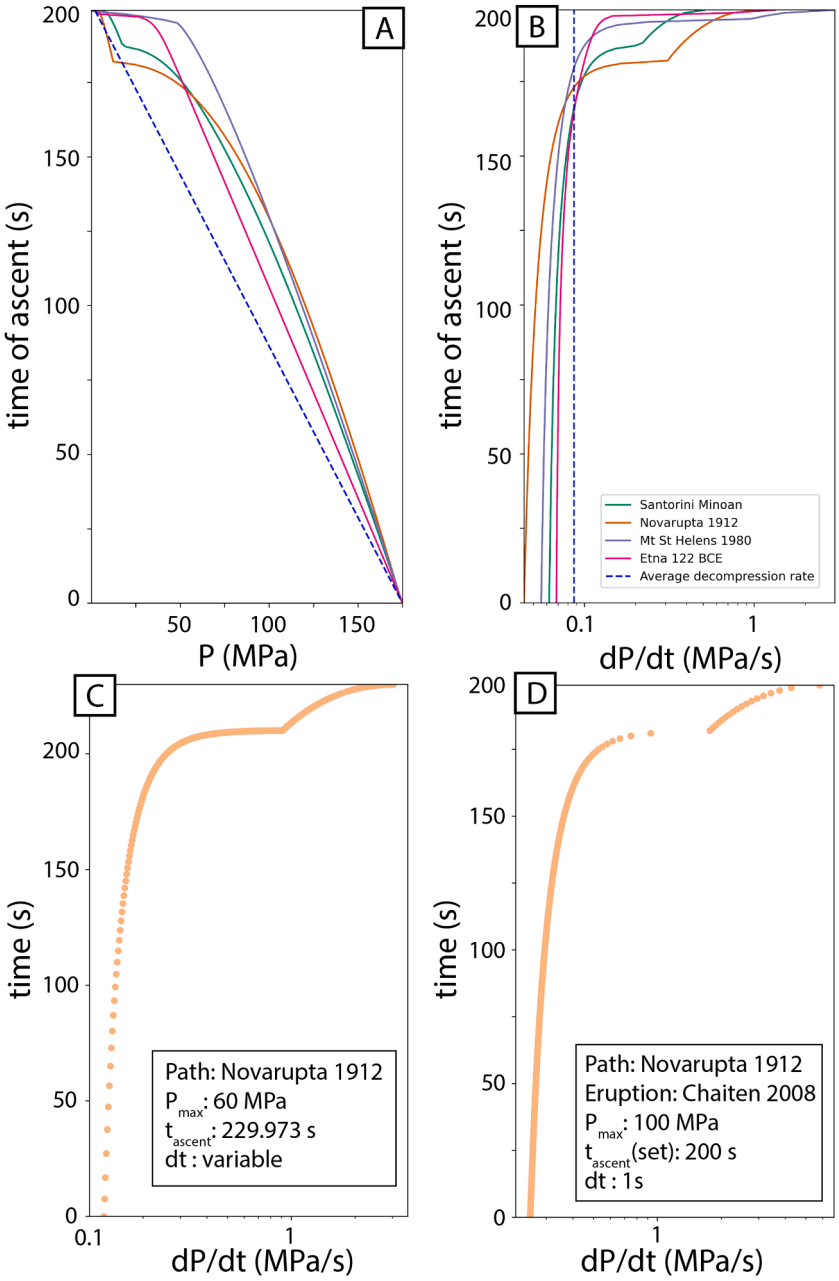

Fig. 3. Magma P-t (A), and decompression (B) paths obtained from Confort 15 (Santorini, Novarupta and Mt St Helens) and MAMMA (Etna) models used as reference ascent paths in that paper. All velocity curves have been scaled for a 200 s ascent and a 175 MPa of initial pressure. This is only for the sake of comparison between shapes of the different paths. For calculations, initial pressures and temperatures have been adapted to the eruptions studied (Table 1), where time of decompression was set at 200 s. The blue dotted line represents the average decompression rate of these profiles. (C-D) Example showing how a profile path is adapted and rescaled for another eruption with the Novarupta 1912 ascent path adapted to the Chaiten 2008 eruption conditions. In this example, we "scaled" Novarupta 1912 ascent path using Chaiten's initial and final pressure (Castro and Dingwell, 2009) and the time of ascent set at 200 s. Each individual point is recalculated in order to keep the shape of the ascent path and satisfy the initial conditions (storage pressure and time of ascent) with a constant time step (dt) of 1 s between data points to be used in the diffusion chronometry model.

studies of each eruption (Table 1). From these simulations, we obtained the parameters of interest (i.e., magma decompression rate, pressure, etc., Fig. 3). To obtain a range of magma ascent paths from different eruption scenarios and magma compositions, we run simulations using initial parameters corresponding to four well-studied plinian eruptions from the literature. We chose the Etna 122 BCE eruption (Coltelli et al., 1998; Sable et al., 2006; Arzilli et al., 2019), the Mount St Helens 1980 plinian eruption (Rutherford et al., 1985; Toramaru, 2006), the Santorini Late Bronze Age, 1600 BCE eruption (Druitt, 2014; Myers et al., 2021) and the Novarupta 1912 eruption (Hammer et al., 2002; Adams et al., 2006b, 2006a; Nguyen et al., 2014). Moreover, we used two conduit models: (1) the Fortran based Confort 15 model (Campagnola et al., 2016) which applies to silicic plinian eruption scenarios and is an improved version of the open-source Conflow model (Mastin, 2002); And (2) the Fortran based MAMMA (Magma Ascent Mathematical Modelling and Analysis) model developed by La Spina et al. (2015, 2016) which is a 1D steady-state model for magma ascent in a cylindrical conduit, applicable to mafic and silicic magmas. These two different models were used because the Confort 15 model does not work well to reproduce ascent paths of mafic plinian eruptions (Etna 122 BCE in our case), unlike MAMMA which was produced and tested for this type of eruption.

The output of these models are magma ascent velocity paths throughout the conduit as a function of pressure and ascent time (Fig. 3A–C). Different results are obtained depending on the input parameters (Campagnola et al., 2016; La Spina et al., 2021; Bamber et al., 2022), such as storage pressure and temperature, initial volatile content and conduit diameter. In principle, it is useful to perform a sensitivity analysis to estimate the influence of each input parameter on the outputs (La Spina et al., 2021). However, here we are more concerned by capturing a "representative" decompression path for different end-member scenarios rather than focussing on a single eruption in detail, and thus we did not perform any sensitivity analysis.

The magma velocity paths were used to obtain time vs volatile concentration in the melt for non-linear decompression scenarios. To do this, for each eruption, we calculate the saturation of volatile at each of the non-linear pressure steps with MagmaSat. Each of these pressure steps have a corresponding time as it is linked to a magma velocity path, allowing us to convert these non-linear pressure vs volatile concentration paths into time vs volatile concentration paths (Fig. 2a–c). We did not simulate all the 13 studied eruptions, instead we used the four eruption paths described above as references and adjusted the initial pressure, time of ascent and average ascent velocities to match the eruptions of interest (Table 1) while keeping the overall path shapes (Fig. 3C, D). We used literature data for each eruption to derive a magma storage pressure (*Pi*), whereas final pressure (*Pf*) was set as the atmospheric pressure (Table 1). Velocity was also proportionally adjusted to fit a given time of ascent, which we chose to be the same for all eruptions to have a common ground of comparison. We repeated this process to create velocity profiles based on conduit models of different eruption scenarios in order to characterise the influence of the shape of the magma ascent path on the boundary condition for the diffusion chronometry models.

2.7. Comparison between the different boundary conditions

To compare the effects of constant versus non-linear decompression rate scenarios, we initially use the same time for both in the forward modelling of volatile reequilibration in melt embayments. The calculated diffusion profiles were then compared by using the profile from the non-linear decompression as a reference and the constant decompression profile as a match for different times (Fig. 4; i.e. we vary the time of diffusion for the constant model to best fit the non-linear model). To obtain a best fit we use the least-squares method to minimise the difference between the two profiles. The time from the best match of the constant decompression was compared to that of the non-linear decompression.

3. Results

3.1. Details of the magma ascent scenarios

We used 4 ascent scenarios (Fig. 3A, B), that corresponds to 4 eruptions that have different magma ascent paths. All ascent scenarios where obtained using initial parameters of Plinian eruptions of various volcanic explosivity indices (VEIs; Etna 122 BCE: VEI-5; Mt St Helens 1980: VEI-5; Novarupta 1912: VEI-6; Santorini Minoan: VEI-7; Global Volcanism Program) and magma composition ranging from basaltic to rhyolitic. These paths have not been calibrated to be as close as possible to what we think were the conditions of ascent of these 4 eruptions but are supposed to be representative of a range of ascent conditions. Etna 122 BCE ascent path follows a steadily accelerating trend until it reaches fragmentation very close to the surface. In contrast, Mt St Helens ascent path shows a sharp increase prior to fragmentation which occurs relatively deep compared to the other ascent paths. All paths are curved with kinks, which is characteristic of fragmentation at low pressure. The position in depth and time of this kink varies between profiles with Novarupta displaying the earliest fragmentation during ascent, followed by Santorini, Mount St Helens and then Etna (Fig. 3B). The shape of each ascent path is linked to the starting conditions of the conduit simulations

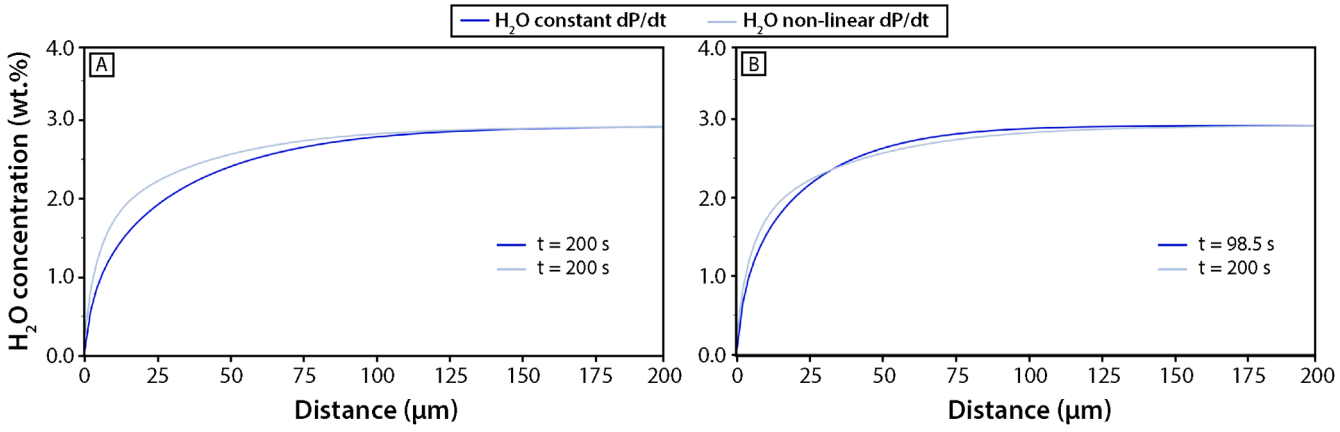

Fig. 4. Effect of the boundary condition (BC) on the diffusion profile of a simulated melt embayment, example of Etna 122 BCE eruption velocity profile and initial parameters. A) Comparison of same duration diffusion profiles for constant decompression vs non-linear decompression BCs. B) Least-square best fit of the non-linear BC diffusion profile by the constant BC diffusion profile. To achieve a fit between the two, time had to be halved for the constant diffusion profile, implying a two-fold increase in the corresponding decompression-rate.

(conduit diameter, bubble number density, melt composition, initial volatile content, pressure and temperature, etc.). These conditions are reported in supplementary material. One of the main differences in the ascent path shapes relates to the degree of non-linearity (λ) close to the surface, which was described by Su and Huber (2017) from their Eq. (1). Mount St Helens ascent path has the highest degree of non-linearity with a brutal acceleration in the last seconds of ascent (Fig. 3A), while on the opposite side of the spectra, Novarupta and Santorini have more gradual accelerations until fragmentation. Etna shows an in-between behaviour.

3.2. Effect on the diffusion profile shape

We modelled diffusion profiles in melt, based on the saturation profiles obtained from MagmaSat (Fig. 5), to simulate the natural profiles measured in melt embayments. We found that the shapes of the water diffusion profiles in the melt produced from constant and non-linear decompression rate models are different (Fig. 6). Constant rate models give smoother changes in gradients, whereas the increasing decompression rate models produce larger changes in the compositional gradient towards the boundary (increasing slope towards the margin). This is due to a more progressive decrease in H_2O during ascent in the case of a constant decompression rate compared to a steeper decrease in H_2O at low pressure for an accelerating non-linear decompression rate (Figs. 5 and 6). For CO_2, there is a similar phenomenon to water, albeit less visible due to the CO_2 concentration decrease in the melt occurring mostly at depth, where decompression rates in the non-linear case scenario are slower (Fig. 5).

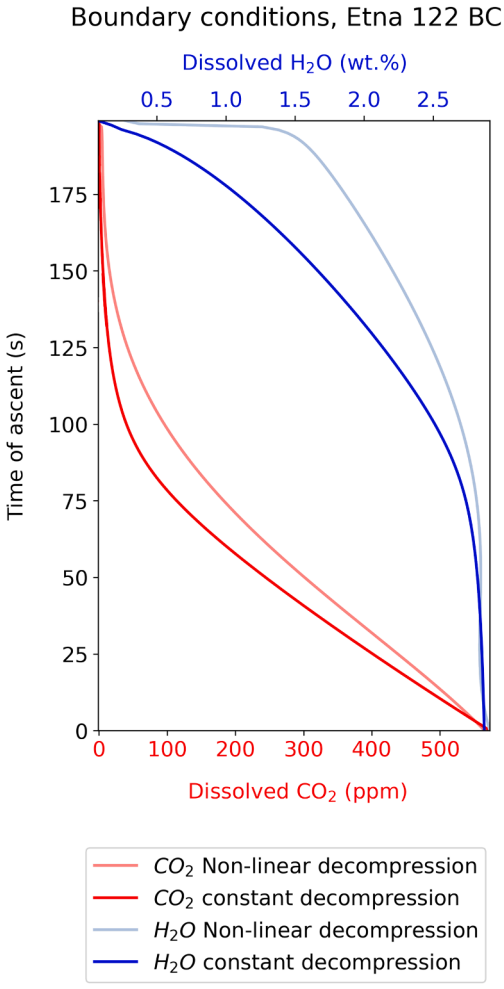

Fig. 5. MagmaSat (Ghiorso and Gualda, 2015) H_2O (blue) and CO_2 (red) saturation models used as boundary conditions in the diffusion chronometry model of the simulated melt embayment. The chosen case study here is the Etna 122 BCE eruption for a time of ascent of 200 s. The darker profiles correspond to constant dP/dt and the light profiles correspond to non-linear dP/dt. We can see that the dissolved volatile content stays higher (with stronger effect for H_2O) at a given time of ascent, with a steeper decrease closer to the end of the ascent for H_2O.

3.3. The effect of constant vs non-linear decompression

The average decompression rates were compared between the two scenarios of constant and non-linear decompression boundary conditions (Fig. 7, Table 2). For H_2O diffusion, the average non-linear decompression rate tends to be smaller than the constant decompression rate; the difference varies from negligible to a factor of 3 to 7 for the Llaima Curacautin eruption if we apply two different velocity paths (Etna 122 BCE or Mt St Helens 1980; Table 2, Fig. 7). The effect is much stronger for mafic and hotter eruptions than for cooler and more silica-rich magmas which show < 25 % relative difference between constant and non-linear decompression.

The CO_2 shows a lesser effect on decompression rate variation than H_2O. For plinian eruptions fed by cold felsic magmas, the average decompression rate estimation from diffusion modelling in the melt embayment increases by 10–60 % when using a constant decompression rate vs a non-linear decompression rate. In general, eruptions that were the least affected by H_2O are now the one the most affected. Overall, CO_2 has a less significant effect on whether a non-linear or constant decompression rate is used than H_2O, with variation of a factor of up to 6 when we consider only water and a variation of up to 0.6 when we consider CO_2. For H_2O and the examples considered, the intermediate to felsic magmas vary between a factor of 0.95 to 1.75 variation in dP/dt, while for mafic hot composition it varies from 0.85 to 6.

For a given eruption, we obtain different best fit dP/dt depending on the magma reference ascent path that we use. For instance, for the Pinatubo 1991 eruption, the average decompression rate obtained by diffusion chronometry using 200 s of ascent and a starting pressure of 220 MPa (Table 1) is 1.1 MPa/s. When the Novarupta 1912 reference decompression path is used, for H_2O we obtain a best fit of the constant model to the reference path at 0.95 MPa/s, while for CO_2 it stands at 0.48 MPa/s. If the Mt St Helens 1980 reference path is used, for H_2O, we obtain a best fit of the constant model to the reference path at 1.42 MPa/s, while for CO_2 it stands at 0.45 MPa/s (Fig. 7).

4. Discussion

4.1. Interpretation of the results

The overall implication of these results is that the boundary condition of the H_2O and CO_2 in the external melt (e.g., how the volatile concentrations change with time and pressure) significantly influences the timescales obtained from diffusion chronometry and, consequently, the inferred decompression rates. This effect also, to a lesser extent, impacts the shapes of the diffusion profiles. For the case studies we investigated, this effect is much stronger for H_2O than for CO_2, with a decrease in the average decompression rates by up to a factor of 7 when comparing constant and non-linear decompression rate models.

4.1.1. Influence of the shape of magma ascent paths

The estimated magma decompression rate from diffusion modelling is highly dependent on the type of magma ascent path used to model non-linear boundary conditions. For instance, the Llaima Curacautin case study using the Mt St Helens 1980 reference ascent path gives decompression rates that are about a factor of 7 slower than a linear boundary, whereas using the Novarupta 1912 reference ascent path gives decompression rates slower by a factor of 1.3 (Fig. 7). Overall, we find that mafic magmas show a higher deviation from the constant decompression model with a non-linear ascent path. This effect could

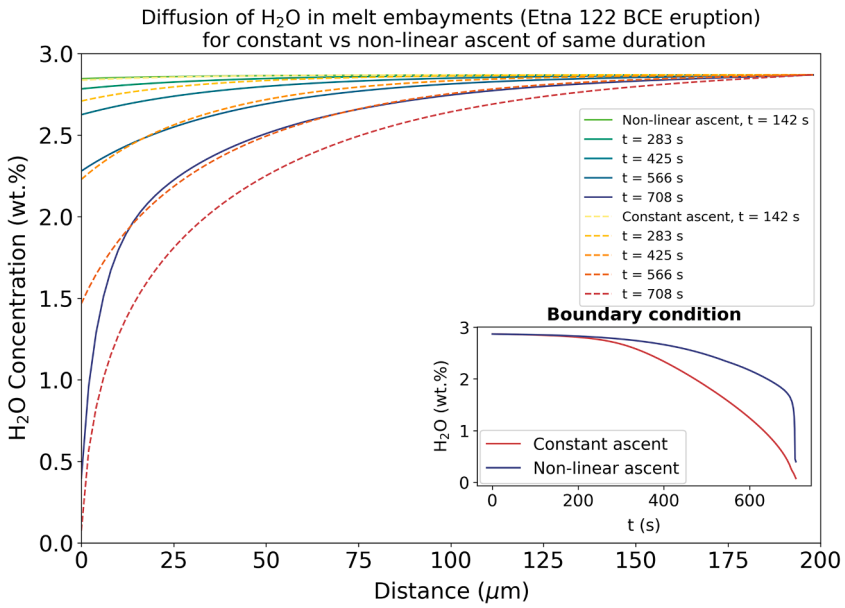

Fig. 6. Evolution of the H_2O in melt diffusion profile for a constant decompression vs a non-linear decompression. The non-linear boundary condition results in a steeper slope towards the boundary compared with the constant boundary condition, with overall more H_2O remaining in the melt for in the non-linear case at a given distance compared to the constant case.

potentially be linked to higher diffusivity of H_2O and CO_2 at higher temperature. However, there is also most likely an effect of the higher starting pressure for the simulation, which implies faster average decompression rate as all our simulations are fixed at 200 s of ascent. This shows that it is important to choose a magma ascent path corresponding to the style of the eruption or make a conduit model based on the known parameters of the studied eruption.

From the ranges of magma ascent paths that we used, those of the Mt St Helens 1980 and Etna 122 BCE have the most significant drops in dP/dt towards the end of the ascent, with a magma acceleration occurring close to the surface (see Fig. 3B). Such a late and abrupt pressure drop gives less time for dissolved volatiles in the magma to exsolve and reequilibrate. Such an effect would be magnified if we applied a delay for the volatile reequilibration to simulate disequilibrium degassing, as may be the case in nature (Mangan and Sisson, 2000). Other magma ascent paths such as the Novarupta 1912 reference show a more gradual acceleration, and applying a constant decompression rate hypothesis at the boundary for diffusion chronometry affects much less the calculated dP/dt values (a factor of less than 1.5).

These results agree with those of Su and Huber (2017), who showed that constant decompression rates tended to underestimate calculated ascent times. They also found that the higher the nonlinearity of the ascent path (λ parameter in their study) the more magma ascent time were underestimated with a constant ascent rate hypothesis. In addition, Barth et al. (2019), also highlighted this ascent time underestimation with greater non-linearity of the ascent path and also the importance to couple diffusion and conduit models.

4.1.2. *The contrasting effect of H_2O vs CO_2*

The effect of using a non-linear ascent rate vs a constant one as the boundary condition is very different depending on whether H_2O or CO_2 are used to infer the times. This is mostly due to their different solubility properties in the magma. CO_2 is much less soluble than H_2O and thus it begins to exsolve deeper than H_2O (Fig. 5), and its concentration in the melt decreases early during ascent which results in a smaller influence of the type of boundary condition used for diffusion chronometry. On the other hand, H_2O is more influenced as its concentration changes significantly during most part of the magma ascent, with the larger change occurring in the shallowest part of the conduit, where acceleration is the largest in case of a non-linear magma ascent.

4.1.3. *Significance of the diffusion profile shape*

We show that there is a significant difference in diffusion profile shape whether we are in a case of constant or non-linear decompression rate (Figs. 4 and 6). This shape may be a good indication to discriminate between the type of boundary condition that needs to be used when fitting natural diffusion profiles. Fig. 6 shows that for a diffusion time of 700 s, we can expect 0.7 wt.% more H_2O at 25 μm from the bubble for a non-linear decompression rate compared to a constant decompression rate. Overall, we observed that the diffusion profiles resulting from accelerating magma decompression rate were enriched in H_2O at a given distance to the vesicle, which resulted in steeper slopes of the diffusion profiles towards the vesicle. Practically, to see this shape in natural data, we should focus on improving our spatial resolution when measuring H_2O in glass in the closest 20–50 μm to the bubble. This effect would also exist when measuring H profiles in nominally anhydrous minerals (H in Olivine for example) but would not be seen in species that diffuses early in the ascent such as CO_2.

4.1.4. *Effect of temperature and boundary condition*

Temperature has a major effect on diffusion coefficient and thus its uncertainty is often considered in the uncertainty of the obtained times (e.g. Costa 2021). To compare the effect of temperature uncertainty with that of the non-linear boundary condition, we calculated a constant decompression rate diffusion profile with a $T = 850 \pm 50$ °C uncertainty on temperature with the non-linear decompression rate diffusion profile without uncertainty on temperature. For the case of H_2O diffusion in embayment and taking the Etna 122 BCE eruption as reference ascent path (Fig. S2), we find that such a variation in temperature (100 °C) would have a similar impact on the diffusion profile compared to using a non-linear boundary condition. For CO_2, the effect of temperature is more important than the boundary condition.

Finally, we also tested a non-linear temperature decrease, which can be implemented easily with the use of a non-linear decompression boundary hypothesis. Temperature is traditionally considered constant during the time of ascent for diffusion modelling studies and equal to the storage temperature, except for a few studies where thermal histories of the system is constrained (Newcombe et al., 2020b). However, conduit

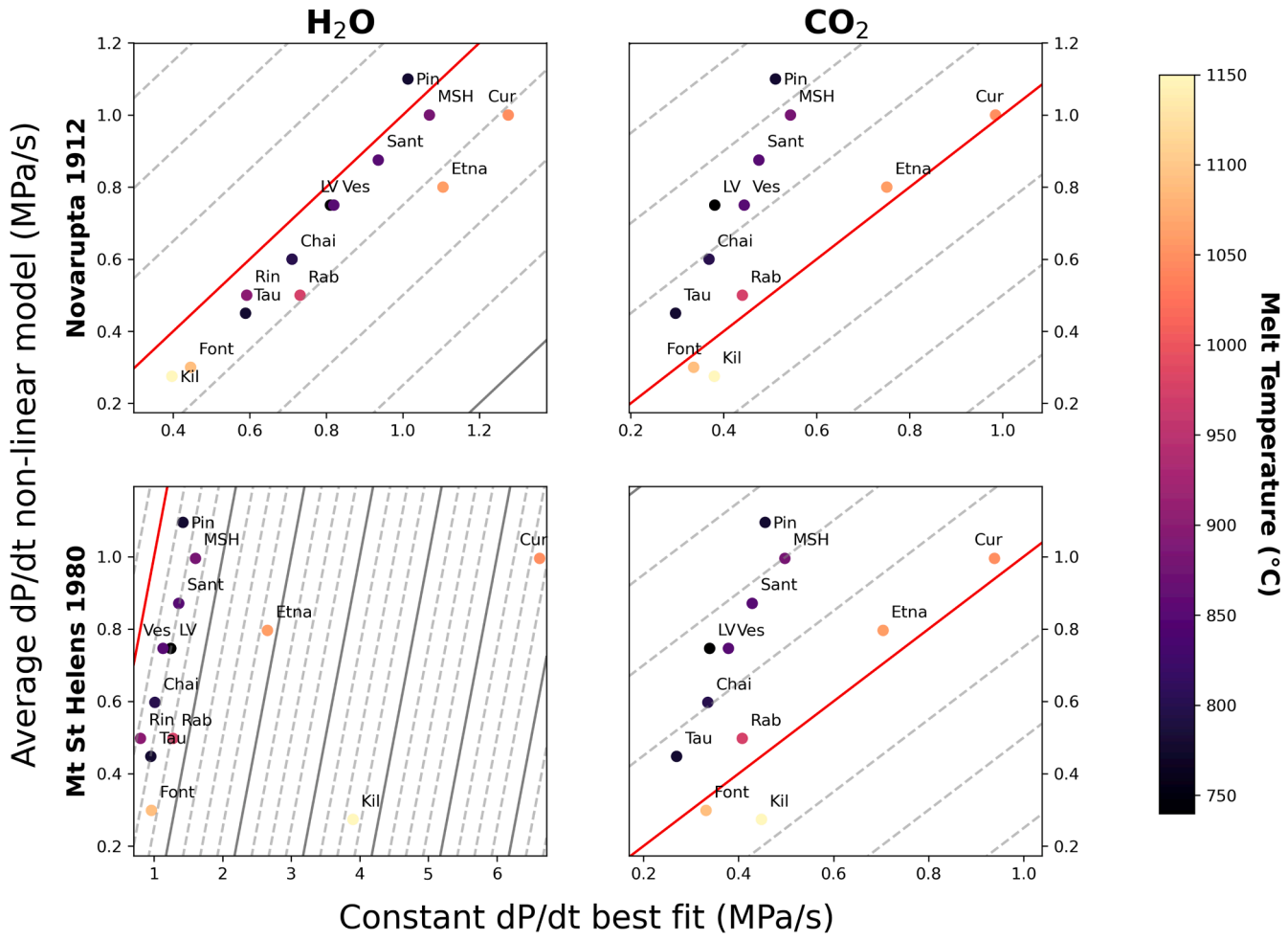

Fig. 7. Comparison of the two types of boundary conditions – the mean of the non-linear decompression rate and the constant decompression rate. Results are for H_2O and CO_2 in the case of forward diffusion modelling of H_2O-CO_2 diffusion in melt embayments. As reference for the non-linear profile, we use the Novarupta 1912 and Mt St Helens 1980 reference ascent paths (additional cases with ascent paths derived from the Santorini 1600 BCE and Etna 122 BCE eruptions are shown in supplementary Fig. S1). The red lines are the 1:1 lines for which the average dP/dt obtained from the diffusion profile with the non-linear boundary condition equals the constant dP/dt used at the constant boundary condition. The grey dotted lines are parallel to the 1:1 red line with equal spacing every 25 % and the grey continuous line represents every 100 % difference to the 1:1 line. Eruptions are color-coded based on their pre-eruptive temperature (Table 1). The eruptions of interests (Kil: Kilauea 1992; Font: Fontana Lapilli, Masaya; Etna: Etna 122 BCE; Cur: Llaima Curacautín; Rab: Rabaul - Tavurvur 2006 sub-plinian eruption phase; Rin: Rinjani 1257 CE; MSH: Mt St Helens 1980 plinian phase; Ves: Vesuvius 79 CE; Sant: Santorini 1600 BCE; Chai: Chaiten 2008 plinian phase; Pin: Pinatubo 1991 plinian phase; Tau: Taupo Oruanui; LV: Long Valley Bishop Tuff) for a common 200 s of ascent.

models have shown that the result of all the thermodynamic reactions occurring during magma ascent (crystallisation, volatile exsolution, pressure drop, volume variations between gas and melt phases, etc.) contribute to a drop in temperature that can be as much as 100 °C for mafic plinian eruptions (La Spina et al., 2015; Arzilli et al., 2019; Bamber et al., 2022). For the case of the Etna 122 BCE eruption, the drop in temperature in our conduit model was about 60 °C with most of it occurring in the last part of the decompression. The effect of this temperature drop on the final diffusion profile is negligible and not even visible if the constant temperature and non-linear temperature profiles are plotted together. Therefore, we consider that this effect of temperature can be ignored compared to the effect of the overall non-linear decompression rate.

4.2. Example with natural data

We tested our modelling approach to fit data from H_2O diffusion chronometry in a plagioclase melt embayment (embayment RDP18RE2) from the 1600 BCE Minoan eruption of Santorini and compare the timescales with results from the literature (Fig. 8 – Myers et al., 2021) . For this, we used the code developed by Hosseini et al. (2023) that we compared with our own developed routine using non-linear decompression conditions at the boundary. We found a difference in ascent time of a factor of 2.26 which corresponds to a slower magma ascent rate with the non-linear decompression path. Using the total change in pressure of dP=175 MPa (Table 1) and the times obtained for the constant and non-linear boundary conditions, we obtain average dP/dt of 1.31 MPa/s and 0.58 MPa/s respectively. This illustrates the importance of considering non-linear decompression rate at the boundary. Such an effect is even more significant for hotter magmas of mafic composition for which a single decompression rate model overestimates magma ascent rates by a factor of at least 2 (Fig. 7, Table 2).

4.3. Implication for future work

This study shows that considering a more realistic volatile change at the boundary of a melt embayment or crystals for modelling diffusion profile can have significant effects on the obtained timescales. This should be considered when modelling any volatile diffusion profile in melt and crystals from volcanic systems when the saturation model of the studied volatile species can be constrained.

In this study we explored the effect of four different non-linear

Table 2
Comparison of obtained dP/dt from the least-square regression of the best fit of the non-linear boundary condition (NL) in the diffusion profile by the constant boundary diffusion profile. These values were obtained from H_2O diffusion, using the Etna 122 BCE reference ascent path for the non-linear boundary condition. The values for CO_2 and the other ascent paths are reported in supplementary material.

Eruption	dP/dt constant (MPa/s)	Average dP/dt Non-linear (MPa/s)	dPdtcste/ dPdtNL
Kilauea 1992	2.0	0.27	7.1
Etna 122 BCE	1.4	0.80	1.7
Masaya 60 ka BP	0.55	0.30	1.9
Llaima 13.3 ka BP	3.0	1.0	3.0
Vesuvius 79 AD	0.81	0.75	1.1
Rabaul 2006	0.80	0.50	1.6
Samalas 1257 CE	0.59	0.50	1.2
Santorini 3600 BP	0.95	0.87	1.1
Mt St Helens 1980	1.1	1.0	1.1
Chaiten 2008	0.73	0.60	1.2
Pinatubo 1991	1.0	1.1	0.94
Long Valley 760 ka BP	0.85	0.75	1.1
Taupo 25.7 ka BP	0.61	0.45	1.4

reference ascent paths, with timescales of ascent varying from a factor of 1.5 to 7 depending on the chosen path. For future studies, a wider variety of ascent paths could be used. One way would be to parameterize a large number of ascent paths and use them to fit natural data in order to constrain a range of potential ascent profiles from the best fitting ones. Another aspect could be to build an accurate conduit model for the eruption of interest based on petrological parameters (P, T, X, volatile content, etc.) and use it to fit natural data.

We also showed that one way to distinguish between non-linear and constant decompression in natural data is a high instrumental resolution when measuring volatile concentration close to the outside boundary (bubble or crystal border) to better capture the shape of the diffusion profile. Steep gradients in the diffusion profiles are likely the result of accelerating magma decompression.

Another way to track changes in magma decompression rate is to use diffusion chronometry with different volatile species. Here we showed that CO_2 could give information on deep ascent rates while H_2O on shallow processes. It is also possible to combine timescales from the diffusion of one element (H_2O) in different systems to assess different times of the ascent (Lloyd et al., 2014). Adding other volatiles such as S or Cl, would give yet another perspective for a more realistic understanding of magma ascent. This approach is already being tested by combining different methods to extract magma ascent rate, for instance by combining microlite number density water exsolution rate meter (Toramaru et al., 2008) with H_2O diffusion chronometry in embayment to probe the deep and shallow part of the ascent (Harris et al., 2024).

Therefore, we suggest two main approaches: (1) considering both constant and non-linear decompression rate to test the importance of the boundary condition for the studied samples, and (2) measuring and modelling as many diffusion profiles as possible for various phases to better constrain the range of dP/dt in an eruption. We have shown (Fig. 1) that different crystals or melt pockets may not register the same decompression rates, and a range of results from them would be statistically more informative on the physical processes occurring during magma ascent than those from a single phase/melt/crystal.

Finally, combining diffusion modelling with conduit modelling is a good approach to add some physical meaning to the timescales we obtain. This coupling would help to better inform conduit models with natural data, and allow better testing if our physical models of eruptions truly apply and are detailed enough to explain natural data. Having more accurate and physically constrained timescales would be of great help to models used to make probabilistic scenarios of eruptions at a given volcanic system for crisis management and response.

5. Conclusion

Integration of diffusion chronometry with magma ascent simulations

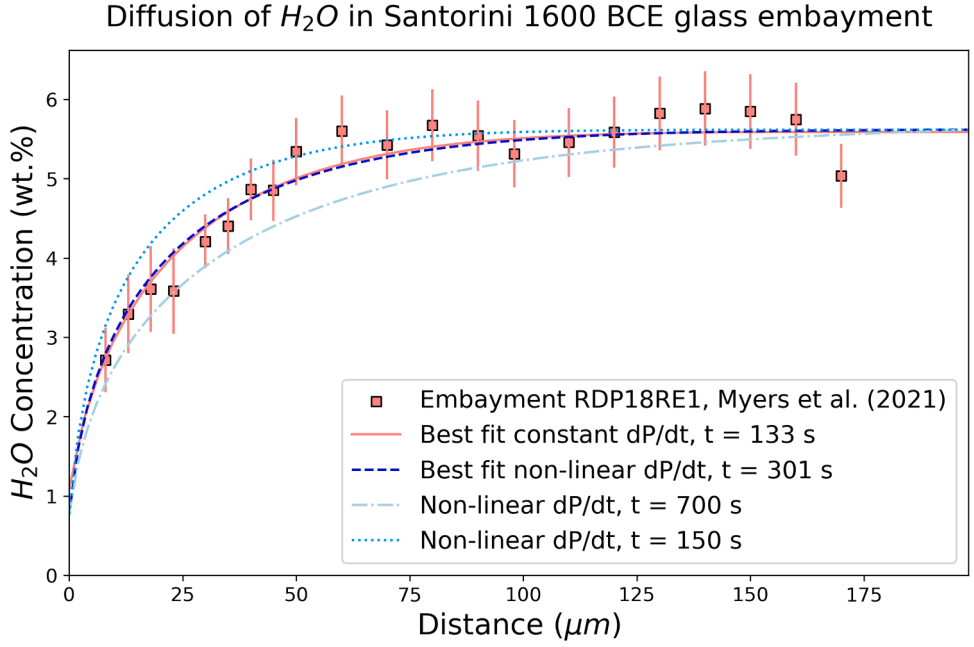

Fig. 8. Natural data from the plagioclase embayment RDP18RE1 from the 1600 BCE eruption of Santorini collected by Myers et al. (2021). The red fit corresponds to the best-fit found by Myers et al. (2021) using a volatile saturation model based on a constant decompression rate as a boundary condition. The blue fit is found using a non-linear decompression rate boundary condition on which a MagmaSat saturation model corresponding to the Santorini 1600 BCE eruption was projected. These parameters were then used to run the diffusion model (see Table 1). The time t in the legend, corresponds to the total diffusion time necessary to obtain the fits with both methods.

shows that non-linear magma ascent can have a significant effect on the inferred decompression rates from diffusion profiles of H_2O and CO_2 in glass and/or crystals. Incorporating a non-linear boundary condition can give a time estimate up to a factor of 7 slower compared to a constant boundary. This change is highly dependent on the magma ascent path, with steeper acceleration of magma decompression rate close to the surface having a large influence. Besides, the shape of the measured diffusion profiles can be a good indicator of whether the magma decompression rate was constant or accelerating with a distinct steeper decrease in H_2O content close to the outside boundary (bubble or crystal border) in the case of non-linear ascent. This type of ascent path can be detected by high-resolution measurement of H_2O in the closest 10 s of micrometres of the outside boundary. In addition, magma decompression rates calculated from CO_2 diffusion chronometry in melt embayments will hardly be affected by the change in boundary condition, while estimates from H_2O diffusion chronometry in melt embayments will be greatly affected. This process is not only restricted to embayment diffusion chronometry, but should be considered when calculating magma decompression rate from diffusion of any volatile species in melt and crystals.

CRediT authorship contribution statement

O. Bernard: Writing – review & editing, Writing – original draft, Visualization, Validation, Project administration, Methodology, Investigation, Formal analysis, Data curation, Conceptualization. **F. Costa:** Writing – review & editing, Validation, Supervision, Project administration, Methodology, Investigation, Funding acquisition.

Declaration of competing interest

The authors declare that they have no known competing financial interests or personal relationships that could have appeared to influence the work reported in this paper.

Acknowledgments

This work greatly benefited from interactions with Giuseppe La Spina on magma ascent modelling and Madison Myers and Behnaz Hosseini on diffusion modelling in embayments. We would also like to thank Weiran Li for her insightful comments on the draft of this manuscript, Terry Plank and an anonymous reviewer for the constructive journal reviews, and Chiara Petrone for editing this work. We acknowledge the Institut de Physique du Globe de Paris and the Université Paris Cité for funding this research (Chaire d'excellence project awarded to Fidel Costa).

Supplementary materials

Supplementary material associated with this article can be found, in the online version, at doi:10.1016/j.epsl.2024.119099.

Data availability

Data will be made available on request.

References

Adams, N.K., Houghton, B.F., Fagents, S.A., Hildreth, W., 2006a. The transition from explosive to effusive eruptive regime: the example of the 1912 Novarupta eruption, Alaska. GSA Bull. 118, 620–634. https://doi.org/10.1130/B25768.1.

Adams, N.K., Houghton, B.F., Hildreth, W., 2006b. Abrupt transitions during sustained explosive eruptions: examples from the 1912 eruption of Novarupta, Alaska. Bull. Volcanol. 69, 189–206. https://doi.org/10.1007/s00445-006-0067-4.

Alfano, F., Bonadonna, C., Gurioli, L., 2012. Insights into eruption dynamics from textural analysis: the case of the May, 2008, Chaitén eruption. Bull. Volcanol. https://doi.org/10.1007/s00445-012-0648-3.

Arzilli, F., Spina, G.L., Burton, M.R., Polacci, M., Gall, N.L., Hartley, M.E., Genova, D.D., Cai, B., Vo, N.T., Bamber, E.C., Nonni, S., Atwood, R., Llewellin, E.W., Brooker, R.A., Mader, H.M., Lee, P.D., 2019. Magma fragmentation in highly explosive basaltic eruptions induced by rapid crystallization. Nat. Geosci. 12, 1023–1028. https://doi.org/10.1038/s41561-019-0468-6.

Bamber, E.C., La Spina, G., Arzilli, F., de' Michieli Vitturi, M., Polacci, M., Hartley, M.E., Petrelli, M., Fellowes, J., Burton, M., 2022. Basaltic Plinian eruptions at Las Sierras-Masaya volcano driven by cool storage of crystal-rich magmas. Commun. Earth Environ. 3, 1–17. https://doi.org/10.1038/s43247-022-00585-5.

Barth, A., Newcombe, M., Plank, T., Gonnermann, H., Hajimirza, S., Soto, G.J., Saballos, A., Hauri, E., 2019. Magma decompression rate correlates with explosivity at basaltic volcanoes — Constraints from water diffusion in olivine. J. Volcanol. Geotherm. Res. 387, 106664. https://doi.org/10.1016/j.jvolgeores.2019.106664.

Barth, A., Plank, T., Towbin, H., 2023. Rates of dehydration in hydrous, high-Fo, magmatic olivines. Geochim. Cosmochim. Acta 342, 62–73. https://doi.org/10.1016/j.gca.2022.11.009.

Behrens, H., Zhang, Y., Xu, Z., 2004. H_2O diffusion in dacitic and andesitic melts. Geochim. Cosmochim. Acta 68, 5139–5150. https://doi.org/10.1016/j.gca.2004.07.008. Structure and Properties of Siliate Melts and Fluids.

Bernard, O., Bouvet de Maisonneuve, C., 2020. Controls on eruption style at Rabaul, Papua New Guinea – Insights from microlites, porosity and permeability measurements. J. Volcanol. Geotherm. Res. 406, 107068. https://doi.org/10.1016/j.jvolgeores.2020.107068.

Bernard, O., Bouvet de Maisonneuve, C., Arbaret, L., Nagashima, K., Oalmann, J., Prabowo, A., Ratdomopurbo, A., 2022a. Varying processes, similar results: how composition influences fragmentation and subsequent feeding of large pyroclastic density currents. Front. Earth Sci. 10 (Lausanne).

Bernard, O., Li, W., Costa, F., Saunders, S., Itikarai, I., Sindang, M., Bouvet de Maisonneuve, C., 2022b. Explosive-effusive-explosive: the role of magma ascent rates and paths in modulating caldera eruptions. Geology. https://doi.org/10.1130/G50023.1.

Campagnola, S., Romano, C., Mastin, L.G., Vona, A., 2016. Confort 15 model of conduit dynamics: applications to Pantelleria Green Tuff and Etna 122 BC eruptions. Contrib. Mineral. Petrol. 171, 60. https://doi.org/10.1007/s00410-016-1265-5.

Cassidy, M., Cole, P.D., Hicks, K.E., Varley, N.R., Peters, N., Lerner, A.H., 2015. Rapid and slow: varying magma ascent rates as a mechanism for Vulcanian explosions. Earth Planet. Sci. Lett. 420, 73–84. https://doi.org/10.1016/j.epsl.2015.03.025.

Cassidy, M., Manga, M., Cashman, K., Bachmann, O., 2018. Controls on explosive-effusive volcanic eruption styles. Nat. Commun. 9. https://doi.org/10.1038/s41467-018-05293-3.

Castro, J.M., Schipper, C.I., Mueller, S.P., Militzer, A.S., Amigo, A., Parejas, C.S., Jacob, D., 2013. Storage and eruption of near-liquidus rhyolite magma at Cordón Caulle, Chile. Bull. Volcanol. 75, 1–17. https://doi.org/10.1007/s00445-013-0702-9.

Caudron, C., White, R.S., Green, R.G., Woods, J., Ágústsdóttir, T., Donaldson, C., Greenfield, T., Rivalta, E., Brandsdóttir, B., 2018. Seismic amplitude ratio analysis of the 2014–2015 Bár arbunga-Holuhraun Dike propagation and eruption. J. Geophys. Res. Solid Earth 123, 264–276. https://doi.org/10.1002/2017JB014660.

Charlier, B.L.A., Morgan, D.J., Wilson, C.J.N., Wooden, J.L., Allan, A.S.R., Baker, J.A., 2012. Lithium concentration gradients in feldspar and quartz record the final minutes of magma ascent in an explosive supereruption. Earth Planet. Sci. Lett. 319–320, 218–227.

Chen, Y., Provost, A., Schiano, P., Cluzel, N., 2013. Magma ascent rate and initial water concentration inferred from diffusive water loss from olivine-hosted melt inclusions. Contrib. Mineral. Petrol. 165, 525–541. https://doi.org/10.1007/s00410-012-0821-x.

Coltelli, M., Del Carlo, P., Vezzoli, L., 1998. Discovery of a Plinian basaltic eruption of Roman age at Etna volcano, Italy. Geology 26, 1095–1098. https://doi.org/10.1130/0091-7613(1998)026<1095:DOAPBE>2.3.CO;2.

Costa, F., 2021. Clocks in magmatic rocks. Annu. Rev. Earth Planet. Sci. 49, 231–252. https://doi.org/10.1146/annurev-earth-080320-060708.

Costa, F., Dohmen, R., Chakraborty, S., 2008. Time scales of magmatic processes from modeling the zoning patterns of crystals. Rev. Mineral. Geochem. 69, 545–594. https://doi.org/10.2138/rmg.2008.69.14.

Costa, F., Morgan, D., 2010. Time constraints from chemical equilibration in magmatic crystals. Timescales of Magmatic Processes: From Core to Atmosphere. https://doi.org/10.1002/9781444328509.

Costa, F., Shea, T., Ubide, T., 2020. Diffusion chronometry and the timescales of magmatic processes. Nat. Rev. Earth Environ. 1, 201–214. https://doi.org/10.1038/s43017-020-0038-x.

Costantini, L., Houghton, B.F., Bonadonna, C., 2010. Constraints on eruption dynamics of basaltic explosive activity derived from chemical and microtextural study: the example of the Fontana Lapilli Plinian eruption, Nicaragua. J. Volcanol. Geotherm. Res. 189, 207–224. https://doi.org/10.1016/j.jvolgeores.2009.11.008.

Cutler, K.S., Watt, S.F.L., Cassidy, M., Madden-Nadeau, A.L., Engwell, S.L., Abdurrachman, M., Nurshal, M.E.M., Tappin, D.R., Carey, S.N., Novellino, A., Hayer, C., Hunt, J.E., Day, S.J., Grilli, S.T., Kurniawan, I.A., Kartadinata, N., 2022. Downward-propagating eruption following vent unloading implies no direct magmatic trigger for the 2018 lateral collapse of Anak Krakatau. Earth Planet. Sci. Lett. 578, 117332. https://doi.org/10.1016/j.epsl.2021.117332.

Degruyter, W., Bachmann, O., Burgisser, A., Manga, M., 2012. The effects of outgassing on the transition between effusive and explosive silicic eruptions. Earth Planet. Sci. Lett. 349–350, 161–170. https://doi.org/10.1016/j.epsl.2012.06.056.

Druitt, T.H., 2014. New insights into the initiation and venting of the Bronze-Age eruption of Santorini (Greece), from component analysis. Bull. Volcanol. 76, 794. https://doi.org/10.1007/s00445-014-0794-x.

Elms, H.C., Myers, M.L., Nichols, A.R.L., Wallace, P.J., Wilson, C.J.N., Barker, S.J., Charlier, B.L.A., 2023. Pre-eruptive rhyolite magma ascent rate is rapid and independent of eruption size: a case study from Okataina Volcanic Centre, Aotearoa New Zealand. Bull. Volcanol. 85, 20. https://doi.org/10.1007/s00445-023-01630-7.

Endo, E.T., Murray, T., 1991. Real-time Seismic Amplitude Measurement (RSAM): a volcano monitoring and prediction tool. Bull. Volcanol. 53, 533–545. https://doi.org/10.1007/BF00298154.

Ferguson, D.J., Gonnermann, H.M., Ruprecht, P., Plank, T., Hauri, E.H., Houghton, B.F., Swanson, D.A., 2016. Magma decompression rates during explosive eruptions of Kīlauea volcano, Hawaii, recorded by melt embayments. Bull. Volcanol. https://doi.org/10.1007/s00445-016-1064-x.

Garcia, M.O., Pietruszka, A.J., Rhodes, J.M., Swanson, K., 2000. Magmatic processes during the prolonged Pu'u 'O'o eruption of Kilauea Volcano, Hawaii. J. Petrol. 41, 967–990. https://doi.org/10.1093/petrology/41.7.967.

Geschwind, C.H., Rutherford, M.J., 1995. Crystallization of microlites during magma ascent: the fluid mechanics of 1980-1986 eruptions at Mount St Helens. Bull. Volcanol. 57, 356–370. https://doi.org/10.1007/BF00301293.

Geshi, N., Yamasaki, T., Miyagi, I., Conway, C.E., 2021. Magma chamber decompression during explosive caldera-forming eruption of Aira caldera. Commun. Earth Environ. 2, 1–10. https://doi.org/10.1038/s43247-021-00272-x.

Ghiorso, M.S., Gualda, G.A.R., 2015. An H2O–CO2 mixed fluid saturation model compatible with rhyolite-MELTS. Contrib. Mineral. Petrol. 169, 53. https://doi.org/10.1007/s00410-015-1141-8.

Gonnermann, H.M., Manga, M., 2013. Dynamics of magma ascent in the volcanic conduit. Modeling Volcanic Processes: The Physics and Mathematics of Volcanism. https://doi.org/10.1017/CBO9781139021562.004.

Hajimirza, S., Gonnermann, H.M., Gardner, J.E., 2021. Reconciling bubble nucleation in explosive eruptions with geospeedometers. Nat. Commun. 12, 283. https://doi.org/10.1038/s41467-020-20541-1.

Hammer, J.E., Rutherford, M.J., 2002. An experimental study of the kinetics of decompression-induced crystallization in silicic melt. J. Geophys. Res. Solid Earth 107. https://doi.org/10.1029/2001JB000281. ECV 8-1-ECV 8-24.

Hammer, J.E., Rutherford, M.J., Hildreth, W., 2002. Magma storage prior to the 1912 eruption at Novarupta, Alaska. Contrib. Mineral. Petrol. 144, 144–162. https://doi.org/10.1007/s00410-002-0393-2.

Harris, M., Hosseini, B., Myers, M., Bouley, L., 2024. Reconciling petrologic magma ascent speedometers for the June 12th, 1991 eruption of Mt. Pinatubo, Philippines. Volcanica 7, 117–133. https://doi.org/10.30909/vol.07.01.117133.

Hildreth, W., Wilson, C.J.N., 2007. Compositional zoning of the Bishop Tuff. J. Petrol. 48, 951–999. https://doi.org/10.1093/petrology/egm007.

Hosseini, B., Myers, M.L., Watkins, J.M., Harris, M.A., 2023. Are we recording? Putting embayment speedometry to the test using high pressure-temperature decompression experiments. Geochem. Geophys. Geosyst. 24. https://doi.org/10.1029/2022GC010770 e2022GC010770.

Houghton, B.F., Carey, R.J., Cashman, K.V., Wilson, C.J.N., Hobden, B.J., Hammer, J.E., 2010. Diverse patterns of ascent, degassing, and eruption of rhyolite magma during the 1.8ka Taupo eruption, New Zealand: evidence from clast vesicularity. J. Volcanol. Geotherm. Res. https://doi.org/10.1016/j.jvolgeores.2010.06.002.

Humphreys, M.C.S., Menand, T., Blundy, J.D., Klimm, K., 2008. Magma ascent rates in explosive eruptions: constraints from H2O diffusion in melt inclusions. Earth Planet. Sci. Lett. 270, 25–40. https://doi.org/10.1016/j.epsl.2008.02.041.

Kozono, T., Koyaguchi, T., 2009. Effects of relative motion between gas and liquid on 1-dimensional steady flow in silicic volcanic conduits: 2. Origin of diversity of eruption styles. J. Volcanol. Geotherm. Res. 180, 37–49. https://doi.org/10.1016/j.jvolgeores.2008.11.007.

La Spina, G., Arzilli, F., Llewellin, E.W., Burton, M.R., Clarke, A.B., de' Michieli Vitturi, M., Polacci, M., Hartley, M.E., Di Genova, D., Mader, H.M., 2021. Explosivity of basaltic lava fountains is controlled by magma rheology, ascent rate and outgassing. Earth Planet. Sci. Lett. 553, 116658. https://doi.org/10.1016/j.epsl.2020.116658.

La Spina, G., Burton, M., de' Michieli Vitturi, M., 2015. Temperature evolution during magma ascent in basaltic effusive eruptions: a numerical application to Stromboli volcano. Earth Planet. Sci. Lett. 426, 89–100. https://doi.org/10.1016/j.epsl.2015.06.015.

La Spina, G., Burton, M., de' Michieli Vitturi, M., Arzilli, F., 2016. Role of syn-eruptive plagioclase disequilibrium crystallization in basaltic magma ascent dynamics. Nat. Commun. 7, 13402. https://doi.org/10.1038/ncomms13402.

Li, W., Chakraborty, S., Nagashima, K., Costa, F., 2020. Multicomponent diffusion of F, Cl and OH in apatite with application to magma ascent rates. Earth Planet. Sci. Lett. 550, 116545. https://doi.org/10.1016/j.epsl.2020.116545.

Liu, Y., Anderson, A.T., Wilson, C.J.N., 2007. Melt pockets in phenocrysts and decompression rates of silicic magmas before fragmentation. J. Geophys. Res. 112, 1–12. https://doi.org/10.1029/2006JB004500.

Liu, Y., Zhang, Y., Behrens, H., 2005. Solubility of H_2O in rhyolitic melts at low pressures and a new empirical model for mixed H_2O–CO_2 solubility in rhyolitic melts. J. Volcanol. Geotherm. Res. 143, 219–235. https://doi.org/10.1016/j.jvolgeores.2004.09.019. Volcanic Eruption Mechanisms.

Lloyd, A.S., Ruprecht, P., Hauri, E.H., Rose, W., Gonnermann, H.M., Plank, T., 2014. NanoSIMS results from olivine-hosted melt embayments: magma ascent rate during explosive basaltic eruptions. J. Volcanol. Geotherm. Res. 283, 1–18. https://doi.org/10.1016/j.jvolgeores.2014.06.002.

Mangan, M., Sisson, T., 2000. Delayed, disequilibrium degassing in rhyolite magma: decompression experiments and implications for explosive volcanism. Earth Planet. Sci. Lett. 183, 441–455. https://doi.org/10.1016/S0012-821X(00)00299-5.

Marshall, A.A., Brand, B.D., Martínez, V., Bowers, J.M., Walker, M., Wanless, V.D., Andrews, B.J., Manga, M., Valdivia, P., Giordano, G., 2022. The mafic Curacautín ignimbrite of Llaima volcano, Chile. J. Volcanol. Geotherm. Res. 421, 107418. https://doi.org/10.1016/j.jvolgeores.2021.107418.

Martel, C., 2012. Eruption dynamics inferred from microlite crystallization experiments: application to plinian and dome-forming eruptions of Mt. Pelée (martinique, lesser antilles). J. Petrol. 53, 699–725. https://doi.org/10.1093/petrology/egr076.

Mastin, L.G., 2002. Insight into volcanic conduit flow from an open-source numerical model. Geochem. Geophys. Geosyst. 3, 519–522. https://doi.org/10.1029/2001GC000192.

Moussallam, Y., Rose-Koga, E.F., Koga, K.T., Médard, E., Bani, P., Devidal, J.-L., Tari, D., 2019. Fast ascent rate during the 2017–2018 Plinian eruption of Ambae (Aoba) volcano: a petrological investigation. Contrib. Mineral. Petrol. 174, 90. https://doi.org/10.1007/s00410-019-1625-z.

Mutch, E.J.F., Maclennan, J., Shorttle, O., Edmonds, M., Rudge, J.F., 2019. Rapid transcrustal magma movement under Iceland. Nat. Geosci. 12, 569–574. https://doi.org/10.1038/s41561-019-0376-9.

Myers, M.L., Druitt, T.H., Schiavi, F., Gurioli, L., Flaherty, T., 2021. Evolution of magma decompression and discharge during a Plinian event (Late Bronze-Age eruption, Santorini) from multiple eruption-intensity proxies. Bull. Volcanol. 83, 18. https://doi.org/10.1007/s00445-021-01438-3.

Myers, M.L., Wallace, P.J., Wilson, C.J.N., 2019. Inferring magma ascent timescales and reconstructing conduit processes in explosive rhyolitic eruptions using diffusive losses of hydrogen from melt inclusions. J. Volcanol. Geotherm. Res. 369, 95–112. https://doi.org/10.1016/j.jvolgeores.2018.11.009.

Myers, M.L., Wallace, P.J., Wilson, C.J.N., Watkins, J.M., Liu, Y., 2018. Ascent rates of rhyolitic magma at the onset of three caldera-forming eruptions. Am. Mineral. 103, 952–965. https://doi.org/10.2138/am-2018-6225.

Newcombe, M.E., Plank, T., Barth, A., Asimow, P.D., Hauri, E., 2020a. Water-in-olivine magma ascent chronometry: every crystal is a clock. J. Volcanol. Geotherm. Res. 398, 106872. https://doi.org/10.1016/j.jvolgeores.2020.106872.

Newcombe, M.E., Plank, T., Zhang, Y., Holycross, M., Barth, A., Lloyd, A.S., Ferguson, D., Houghton, B.F., Hauri, E., 2020b. Magma pressure-temperature-time paths during mafic explosive eruptions. Front. Earth. Sci. 8 (Lausanne).

Newman, S., Lowenstern, J.B., 2002. VOLATILECALC: a silicate melt-H_2O-CO_2 solution model written in Visual Basic for excel. Comput. Geosci. 28, 597–604. https://doi.org/10.1016/S0098-3004(01)00081-4.

Nguyen, C.T., Gonnermann, H.M., Houghton, B.F., 2014. Explosive to effusive transition during the largest volcanic eruption of the 20th century (Novarupta 1912, Alaska). Geology 42, 703–706. https://doi.org/10.1130/G35593.1.

Ostorero, L., Balcone-Boissard, H., Boudon, G., Shapiro, N.M., Belousov, A., Belousova, M., Auer, A., Senyukov, S.L., Droznina, S.Y., 2022. Correlated petrology and seismicity indicate rapid magma accumulation prior to eruption of Kizimen volcano, Kamchatka. Commun. Earth Environ. 3, 1–14. https://doi.org/10.1038/s43247-022-00622-3.

Romano, C., Vona, A., Campagnola, S., Giordano, G., Arienzo, I., Isaia, R., 2020. Modelling and physico-chemical constraints to the 4.5 ka Agnano-Monte Spina Plinian eruption (Campi Flegrei, Italy). Chem. Geol. 532, 119301. https://doi.org/10.1016/j.chemgeo.2019.119301.

Rutherford, M.J., Devine, J.D., 2003. Magmatic conditions and magma ascent as indicated by hornblende phase equilibria and reactions in the 1995–2002 Soufrière Hills Magma. J. Petrol. 44, 1433–1453. https://doi.org/10.1093/petrology/44.8.1433.

Rutherford, M.J., Hill, P.M., 1993. Magma ascent rates from amphibole breakdown : an experimental study applied to the 1980-1986 Mount St . Helens Eruptions. J. Geophys. Res. 98.

Rutherford, M.J., Sigurdsson, H., Carey, S., Davis, A., 1985. The May 18, 1980, eruption of Mount St. Helens: 1. Melt composition and experimental phase equilibria. J. Geophys. Res. Solid Earth 90, 2929–2947. https://doi.org/10.1029/JB090iB04p02929.

Sable, J.E., Houghton, B.F., Del Carlo, P., Coltelli, M., 2006. Changing conditions of magma ascent and fragmentation during the Etna 122 BC basaltic Plinian eruption: evidence from clast microtextures. J. Volcanol. Geotherm. Res. 158, 333–354. https://doi.org/10.1016/j.jvolgeores.2006.07.006.

Shea, T., 2017. Bubble nucleation in magmas: a dominantly heterogeneous process? J. Volcanol. Geotherm. Res. 343, 155–170. https://doi.org/10.1016/j.jvolgeores.2017.06.025.

Shea, T., Hammer, J.E., 2013. Kinetics of cooling- and decompression-induced crystallization in hydrous mafic-intermediate magmas. J. Volcanol. Geotherm. Res. 260, 127–145. https://doi.org/10.1016/j.jvolgeores.2013.04.018.

Shea, T., Houghton, B.F., Gurioli, L., Cashman, K.V., Hammer, J.E., Hobden, B.J., 2010. Textural studies of vesicles in volcanic rocks: an integrated methodology. J. Volcanol. Geotherm. Res. 190, 271–289. https://doi.org/10.1016/j.jvolgeores.2009.12.003.

Su, Y., Huber, C., 2017. The effect of nonlinear decompression history on H_2O/CO_2 vesiculation in rhyolitic magmas. J. Geophys. Res. Solid Earth 122, 2712–2723. https://doi.org/10.1002/2016JB013812.

Thivet, S., Gurioli, L., Di Muro, A., 2020. Basaltic dyke eruptions at Piton de La Fournaise: characterization of the eruptive products with implications for reservoir conditions, conduit processes and eruptive dynamics. Contrib. Mineral. Petrol. https://doi.org/10.1007/s00410-020-1664-5.

Toramaru, A., 2006. BND (bubble number density) decompression rate meter for explosive volcanic eruptions. J. Volcanol. Geotherm. Res. 154, 303–316. https://doi.org/10.1016/j.jvolgeores.2006.03.027.

Toramaru, A., Noguchi, S., Oyoshihara, S., Tsune, A., 2008. MND(microlite number density) water exsolution rate meter. J. Volcanol. Geotherm. Res. 175, 156–167. https://doi.org/10.1016/j.jvolgeores.2008.03.035.

Towbin, W.H., Plank, T., Klein, E., Hauri, E., 2023. Measuring H_2O concentrations in olivine by secondary ion mass spectrometry: challenges and paths forward. Am. Mineral. 108, 928–940. https://doi.org/10.2138/am-2022-8247. Journal of Earth and Planetary Materials.

Valdivia, P., Marshall, A.A., Brand, B.D., Manga, M., Huber, C., 2021. Mafic explosive volcanism at Llaima Volcano: 3D x-ray microtomography reconstruction of pyroclasts to constrain shallow conduit processes. Bull. Volcanol. 84, 2. https://doi.org/10.1007/s00445-021-01514-8.

Wilson, C.J.N., Black, S., Charlier, B.L.A., Sutton, A.N., 2006. The 26·5 ka Oruanui Eruption, Taupo Volcano, New Zealand: development, characteristics and evacuation of a large rhyolitic magma body. J. Petrol. 47, 35–69. https://doi.org/10.1093/petrology/egi066.

Zhang, Y., Behrens, H., 2000. H2O diffusion in rhyolitic melts and glasses. Chem. Geol. 169, 243–262. https://doi.org/10.1016/S0009-2541(99)00231-4.

Zhang, Y., Xu, Z., Zhu, M., Wang, H., 2007. Silicate melt properties and volcanic eruptions. Rev. Geophys. 45. https://doi.org/10.1029/2006RG000216.

Zuccarello, F., Schiavi, F., Viccaro, M., 2022. The eruption run-up at Mt. Etna volcano: constraining magma decompression rates and their relationships with the final eruptive energy. Earth Planet. Sci. Lett. 597, 117821. https://doi.org/10.1016/j.epsl.2022.117821.